Measurements of 525 GeV pion interactions in emulsion

M. L. Cherry, W. V. Jones, K. Sengupta, and J. P. Wefel
Department of Physics and Astronomy, Louisiana State University, Baton Rouge, Louisiana 70803

A. Dąbrowska, R. Hołyński, A. Jurak, M. Szarska, B. Wosiek, and K. Woźniak
Institute of Nuclear Physics, Kawiory 26 A, 30-055, Kraków, Poland

E. Baklickaj, L. P. Chernova, K. G. Gulamov, N. S. Lukicheva, V. Sh. Navotny, N. Sh. Saidkhanov, L. N. Svechnikova, and S. I. Zhochova
Physical-Technical Institute, 700084 Tashkent, Uzbekistan

M. I. Adamovich, M. M. Chernyavski, S. G. Gerassimov, S. P. Kharlamov, V. G. Larionova, G. I. Orlova, N. G. Peresadko, N. A. Salmanova, and M. I. Tretyakova
P. N. Lebedev Physical Institute, 117324 Moscow, Russia
(Received 5 May 1994)

Measurements have been made of inclusive 525 GeV π^- interactions in emulsion. The results are compared to proton-emulsion and lower energy pion-emulsion data. Average multiplicities of relativistic shower particles increase with increasing energy, although with a somewhat steeper slope above 60 GeV than at lower energies. The ratio $\langle n_s \rangle_p / \langle n_s \rangle_\pi \sim 1.1$ over the energy range 60–525 GeV. The ratio of the dispersion in the multiplicity distribution to the average multiplicity is the same for proton and pion collisions in emulsion, and is independent of projectile energy. The shape of the shower particle multiplicity distribution does not vary significantly with energy, and KNO scaling appears to hold over the energy range 60–525 GeV. The shower particle pseudorapidity distributions are independent of the beam energy in the target and projectile fragmentation regions, and both the pseudorapidity and multiplicity distributions agree reasonably well with the FRITIOF model predictions for 525 GeV pions. The dependence of the shower particle multiplicity $\langle n_s \rangle$ on the number of heavy tracks N_h approaches saturation as the total shower particle energy becomes a significant fraction of $\sqrt{s}$, and the pseudorapidity distributions shift toward smaller $\langle \eta \rangle$ with increasing numbers of grey and black tracks at 525 GeV. Neither the average number $\langle N_h \rangle$ nor the multiplicity distributions of the heavily ionizing tracks vary significantly with energy, and the normalized angular distributions of grey and black tracks are independent of the type of projectile or projectile energy.

PACS number(s): 13.85.−t, 25.75.+r, 25.80.Hp

I. INTRODUCTION

Photographic emulsion, with its excellent spatial resolution and high efficiency for the detection of charged particles over the full solid angle range, is especially suitable for studies of high energy interactions. The presence of heavy nuclei in the target allows the possibility of significantly more complicated (and correspondingly interesting) processes than in the collision of a projectile with a single target nucleon. With a heavy target, a projectile may interact with multiple target nucleons, providing a snapshot of the time development of the interaction process. The multiple collisions may lead to the high energy densities required, for example, to create a quark-gluon plasma, especially in heavy ion interactions [1]. Studies of high energy nucleus-nucleus interactions are, so far, consistent with a superposition of individual hadron-nucleus collisions [2]. This conclusion, however, relies on a detailed understanding of the hadron-nucleus interaction processes over a wide range of primary energies.

Previous experiments on hadron-nucleus collisions have been reviewed by Fredricksson *et al.* [3]. We have now extended this series of measurements to pions at 525 GeV, the highest available fixed target energy, and present the 525 GeV results here together with a comparison with earlier pion and proton results [4–12]. The experimental procedures are summarized in Sec. II. In Sec. III, the average shower particle multiplicities and dispersions are given as a function of energy, and the multiplicity distributions are compared to both phenomenological distributions derived from lower energy data and to a negative binomial and log-normal distribution. The shower particle pseudorapidity distributions are also discussed in Sec. III. Section IV is devoted to the study of multiplicity and angular distributions of the heavily ionizing particles in emulsion. The correlation between particle production and fragmentation of the target nucleus are discussed in Sec. V. Finally, we summarize the results and present our conclusions.

II. EXPERIMENTAL PROCEDURE

Stacks of BR-2 emulsion pellicles of dimension 20 cm $\times$ 10 cm $\times$ 600 μm were exposed to a 525 GeV π^- beam at Fermilab (Experiment No. E667). The beam was directed parallel to the surface of the emulsions. Primary interactions were found by along-the-track scanning of the processed emulsion plates under high magnification. A total of 1750 inelastic interactions were obtained after excluding from the sample 138 coherent events using the method described in Ref. [13]. The measured mean free path $\lambda = 40.8 \pm 1.0$ cm agreed well with an optical model calculation [14] of $\lambda = 40.0$ cm performed with the known chemical composition of emulsion as input, and is somewhat shorter than $\lambda = 44.5 \pm 0.3$ cm obtained from the parametrization of Carroll *et al.* [15].

Interactions were analyzed by studying the tracks emitted from the interaction vertices. These tracks were classified according to the commonly accepted emulsion experiment terminology: n_s is the number of shower tracks created by fast particles ($\beta > 0.7$) with ionization $I < 1.4\,I_0$, where I_0 is the ionization due to relativistic particles (~ 27 grains per 100 μm in this experiment); N_g is the number of grey tracks with $1.4\,I_0 < I < 10\,I_0$ (i.e., recoil protons in the kinetic energy range $26 < E < 400$ MeV, with a small number of heavier hydrogen isotopes and a few percent admixture of low-momentum pions); N_b is the number of black tracks with $I > 10I_0$ (singly or multiply charged target fragments with ionization greater than that of a 26 MeV proton).

For the 525 GeV pion analysis, we have made the grey-black identification by measuring the particle range. A 26 MeV proton, leaving in the emulsion a track with $I \sim 10I_0$, has a range of 3 mm. Thus, we have used as a criterion that if a track has residual range ≤ 3 mm, it is black. Grey tracks have range > 3 mm. It should be pointed out that not exactly the same criteria have been applied during the analyses of the other data samples used in this work for comparison, where the classification into grey and black tracks has sometimes been obtained by visual inspection of the track to determine the ionization. Fluctuations in the observed ionization can then lead to uncertainties in the grey-black identification. Given the possibility of systematic differences between grey and black track identification in different data samples using range and ionization measurements, we make no attempt to study the grey and black track energy dependences separately. We do, however, consider the comparison of the number of heavily ionizing tracks N_h, where $N_h = N_g + N_b$, among different data sets. The N_g and N_b tracks are considered separately only in those cases in which the results are not sensitive to the possible biases in $N_g - N_b$ separation.

In each event, the polar angles θ of all shower tracks with respect to the incident particle direction were recorded. Particular attention was given to the smallest angle shower tracks emitted in the very forward direction ($\theta \sim 1$ mrad). The angular measurement of these tracks was made with respect to an appropriately chosen noninteracting beam track, with an accuracy in the angular measurement of 0.1 units of pseudorapidity ($\eta = -\ln\tan\theta/2$). Angles of black and grey tracks were also measured in each event, with an estimated accuracy $\delta\theta \lesssim 1°$.

We have compared the 525 GeV data with the predictions of the Lund Monte Carlo event generator FRITIOF [16]. A sample of 10 000 minimum bias events were generated with FRITIOF using the known chemical composition of BR-2 emulsion.

III. RELATIVISTIC PARTICLES

A. Multiplicity distributions

The mean values $\langle n_s \rangle$ and the dispersions $D(n_s) = (\langle n_s^2 \rangle - \langle n_s \rangle^2)^{1/2}$ are given in Table I for 67–800 GeV protons and 60–525 GeV pions interacting in emulsion [4–12]. Figure 1 shows the mean charged multiplicity of secondary particles $\langle n_s \rangle$ as a function of the beam energy in the lab frame $E_{\rm lab}$ for these high energy minimum bias π and p interactions in emulsion, together with a compilation of data at other energies from Fredriksson *et al.* [3]. A fit of the form $\langle n_s \rangle = a + b \ln E_{\rm lab}$ is shown for the high energy points in Table I, where the values of the parameters a and b are given in Table II. The slopes of the fits to the high energy points are clearly steeper than the trend of the lower energy data. Above 100 GeV, the proton-induced reactions produce $\langle n_s \rangle$ systematically higher than for pions at the same beam energy: The ratio $\langle n_s \rangle_p / \langle n_s \rangle_\pi$ calculated from the parameters in Table II ranges from 1.07 at 67 GeV to 1.15 at 525 GeV. The dispersion is plotted as a function of $\langle n_s \rangle$ for the pion interactions in Fig. 2, where the observed $D(n_s) = (0.14 \pm 0.33) + (0.57 \pm 0.03)\langle n_s \rangle$. The ratio $D/\langle n_s \rangle$ is constant at all energies for both protons and pions, as shown in Table I.

Figure 3 shows the multiplicity distributions for 60, 200, 300, and 525 GeV minimum bias π-emulsion in-

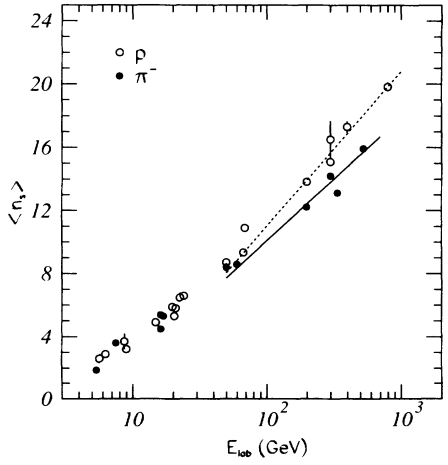

FIG. 1. Average multiplicity vs projectile energy for pion and proton interactions in emulsion. The lines represent fits of the form $a + b \ln E_{\rm lab}$ to the data points above 60 GeV from Table I. Low energy data are taken from Refs. [3–13].

TABLE I. Multiplicity data for shower particles.

Projectile	Energy (GeV/nucleon)	Number of events	$\langle n_s \rangle$	$D(n_s)$	$D/\langle n_s \rangle$
π^-	525	1750	15.93 ± 0.22	9.06± 0.15	0.57± 0.01
π^-	300	2115	14.22 ± 0.18	8.32± 0.14	0.59± 0.01
π^-	200	5785	12.22 ± 0.09	7.13± 0.07	0.58± 0.01
π^-	60	788	8.58 ± 0.18	4.94± 0.14	0.58± 0.02
p	800	1750	19.83 ± 0.29	12.10± 0.19	0.61± 0.01
p	400	854	17.30 ± 0.37	10.72± 0.35	0.60± 0.10
p	200	2595	13.84 ± 0.16	8.32± 0.14	0.60± 0.01
p	67	1183	9.34 ± 0.16	5.63± 0.17	0.62± 0.06

teractions. The lowest energy distribution (60 GeV) is the most sharply peaked; with increasing energy, the position of the maximum increases, the distributions become wider, and the tails grow larger. Figure 4 shows a comparison of the measured 525 GeV shower particle multiplicity distribution with the results of the FRITIOF simulation. The distributions agree reasonably well ($\chi^2/N_{\rm DF} = 2.07$). The average shower particle multiplicity of the Monte Carlo events was 15.91± 0.16, in excellent agreement with the measured value of 15.93± 0.22.

Multiplicity distributions at different beam energies are conveniently compared using the Koba-Nielsen-Olesen (KNO) parametrization [17]. If scaling is valid at high energies, then there exists an energy-independent function $\psi(z)$ satisfying

$$\psi(z) = \langle n_s \rangle P(n_s) = \langle n_s \rangle \sigma_n / \sigma_{\rm inel}, \qquad (1)$$

where $z = n_s/\langle n_s \rangle$ is the shower particle multiplicity normalized by $\langle n_s \rangle$, $P(n_s)$ is the probability of finding n_s charged particles in the final state, σ_n is the cross section for the production of n_s charged particles, and $\sigma_{\rm inel}$ is the total inelastic cross section. KNO scaling has been reported previously in proton-emulsion ($E_{\rm lab} \leq$ 800 GeV [7]) and pion-emulsion ($E_{\rm lab}$ = 60–300 GeV [8]) interactions, although the evidence for KNO scaling in pA interactions is still rather approximate, and the shape of the KNO function seems to depend on the mass number A of the target [3]. Since less is known about the multiplicity distributions from π–A collisions, we have undertaken a systematic study of these distributions for the emulsion target.

Figure 5 shows a plot of $\psi(z)$ as a function of z for π-emulsion interactions at 60, 200, 300, and 525 GeV. The data points corresponding to the different beams fall on top of each other, indicating that scaling occurs at all energies, although the statistical error bars in Fig. 5 may hide small differences among the distributions. The situation may be similar to the hadron-hadron case where KNO scaling appeared to hold through the energy range $2 < \sqrt{s} < 60$ GeV but was clearly violated at higher energies. Whether the same is also true for hadron-nucleus collisions remains to be verified.

Several forms of $\psi(z)$ have been used previously. In Ref. [8] the 60–300 GeV multiplicity data were found to be well represented by the Slattery function

$$\psi(z) = (az + bz^3 + cz^5 + dz^7)\exp(-fz). \qquad (2)$$

In order to test whether the same functional form is a good representation of the 525 GeV data as well, we present in Fig. 6 the $\psi(z)$ versus z plot of the 525 GeV data. The best fit parameters for pion-induced reactions at 525 GeV are $a = 0.95 \pm 0.27$, $b = 35.36 \pm 5.11$, $c = -7.87 \pm 1.37$, $d = 0.97 \pm 0.27$, $f = 3.69 \pm 0.18$, resulting in $\chi^2/N_{\rm DF} = 0.90$. In the same diagram the fit to the 60–300 GeV π^- data of Ref. [8] and the corresponding fit to the 525 GeV data are shown as separate bands. The width of the bands corresponds to varying the individual fit parameters until $\chi^2/N_{\rm DF}$ increases by 1. Overlap of the bands would indicate validity of KNO scaling in the energy range 60–525 GeV. Since the bands in Fig. 6 do not overlap completely, we have performed a Kolmogorov-Smirnov test to determine whether the data sets are consistent with a single distribution function, viz. Eq. (2). We find a significance level of ~ 80%, indicat-

TABLE II. Fit parameters for $\langle n_s \rangle = a + b \ln E_{\rm lab}$.

Projectile	a	b	$\chi^2/N_{\rm DF}$
π	−5.62 ± 0.64	7.84 ± 0.28	6.74
p	−8.59 ± 0.62	9.79 ± 0.28	0.86

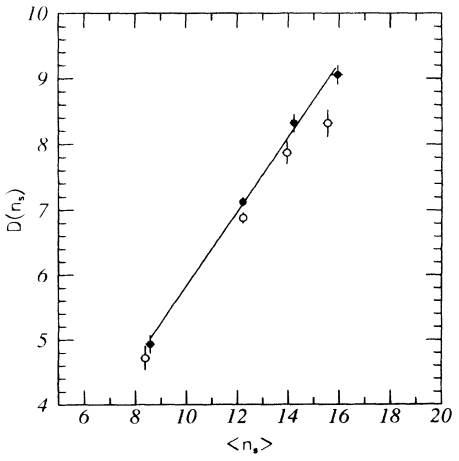

FIG. 2. Dispersion $D(n_s)$ for 60, 200, 300, and 525 GeV pions. Smooth line is straight line fit; open circles represent values calculated from negative binomial fit [Eq. (4)].

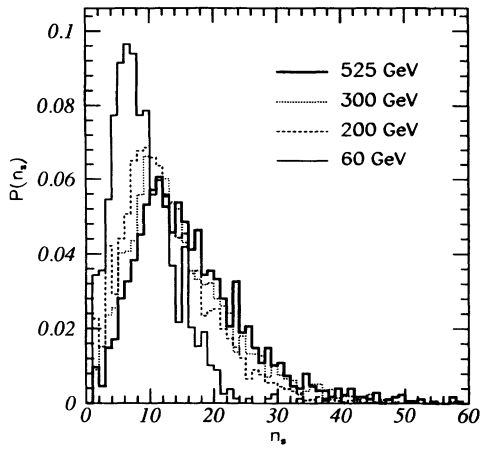

FIG. 3. Shower particle multiplicity distributions for 60–525 GeV pions.

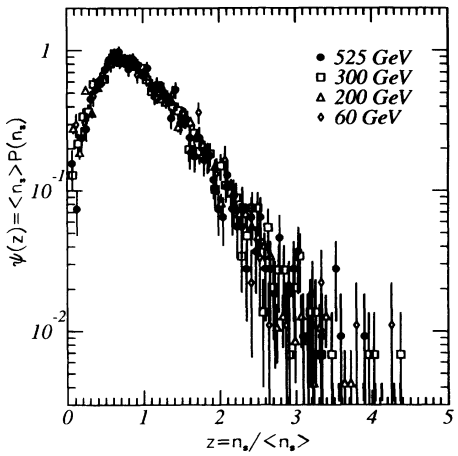

FIG. 5. $\psi(z)$ vs z for 60–525 GeV pions.

ing that the difference between the 525 GeV data and the 60–300 GeV fit is not statistically significant.

We have also compared the measured multiplicity distributions to a negative binomial (NB) distribution

$$P_n^{\mathrm{NB}} = \frac{(n_s+k-1)!}{n_s!(k-1)!}\frac{\langle n_s\rangle^{n_s}k^k}{(\langle n_s\rangle+k)^{n_s+k}} \tag{3}$$

with two free parameters $\langle n_s\rangle$ and k [18]. The parameter k is related to the dispersion D by

$$\frac{D^2}{\langle n_s\rangle^2} = \frac{1}{\langle n_s\rangle} + \frac{1}{k}. \tag{4}$$

Note that for $k = 1$, the NB distribution becomes a simple Bose-Einstein distribution while $k \to \infty$ leads to a Poisson distribution. At high energies, where $\langle n_s\rangle/k \gg 1$, the NB approaches a Γ distribution in the scaled variable $z = n_s/\langle n_s\rangle$:

$$\langle n_s\rangle P_n^G = \frac{k^k}{\Gamma(k)} z^{k-1}\exp(-kz), \tag{5}$$

where k must be independent of energy if KNO scaling is to be valid. In Fig. 7 we show $P(n_s)$ as a function of n_s for the 525 GeV data. The solid line is the result of the negative binomial fit to the data after excluding the first two bins which may be slightly contaminated with diffractive events. The fit parameters for pions at 60–525 GeV and protons at 67–800 GeV are listed in Table III. The χ^2/N_{DF} indicates that the fits to the individual measured distributions are generally satisfactory. In all

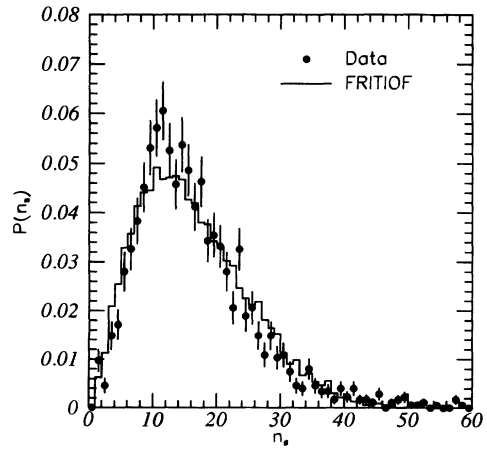

FIG. 4. Measured shower particle multiplicity distribution for 525 GeV pions (•) compared to the predictions of the Monte Carlo code FRITIOF.

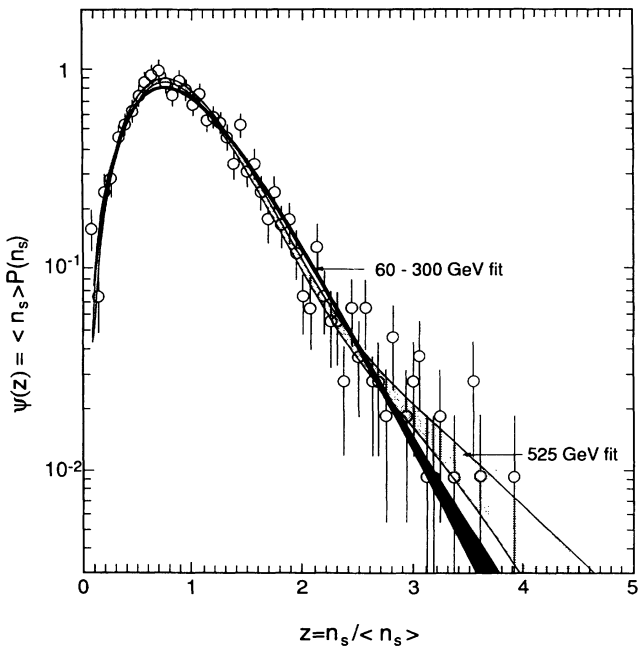

FIG. 6. $\psi(z)$ vs z for 525 GeV pions. The two bands represent fits to the 60–300 GeV π^- data of Ref. [8] and the 525 GeV data of the present work. The width of the bands corresponds to varying the individual fit parameters until χ^2/N_{DF} increases by 1.

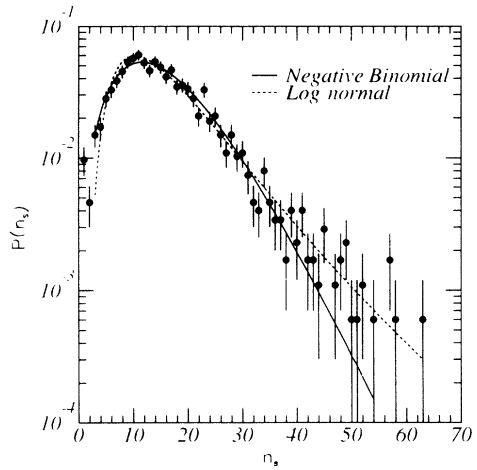

FIG. 7. $P(n_s)$ vs n_s for 525 GeV pions, together with fits to negative binomial and log-normal distributions [Eqs. (3),(6)].

cases, the values of $\langle n_s \rangle$ and $D/\langle n_s \rangle$ obtained from the fitting are within $\sim 10\%$ of the corresponding measured values in Table I, and (with the possible exception of the 60 GeV pion and 67 GeV proton points) the fitted values of k are consistent with a constant value. The values of the NB dispersion, calculated from Eq. (4) and shown as open points in Fig. 2, are systematically $\sim 4\%$ below the best-fit straight line.

A log-normal (LN) distribution for a discrete probability distribution,

$$P_n^{\mathrm{LN}} = \int_{n_s-\frac{1}{2}}^{n_s+\frac{1}{2}} \frac{1}{n\sigma\sqrt{2\pi}} \exp\left(-\frac{(\ln n - \mu)^2}{2\sigma^2}\right) dn, \qquad n_s > 0, \tag{6}$$

with

$$\langle n_s \rangle = \exp(\mu + \sigma^2/2)$$

and

$$D = \langle n_s \rangle [\exp(\sigma^2) - 1]^{1/2} \tag{7}$$

has also been suggested as a simple parametrization of multiplicities in minimum bias hadron-hadron interactions [19,20]. This is a two-parameter statistical probability function that has a simple and appealing physical interpretation: It arises in a multistep cascade process where each step multiplies the previous outcome—a property that gives a natural connection to parton cascades during hadronization. LN distributions have been shown to describe proton data at all available energies (although it has sometimes been necessary to use three fitting parameters instead of just two), including those of the highest energy $p\bar{p}$ interactions at $\sqrt{s} = 900$ GeV, where the NB distribution does not give a good fit [20]. Since nuclear targets are more suitable than protons for the space-time development of a cascade process, it seems reasonable to try a LN parametrization for the present pion-nucleus data as well. The dashed curve in Fig. 7 is the result of such a fit to the 525 GeV pion data (after again excluding the first two bins); the fitted parameters are given in Table IV. At 525 GeV we obtain an excellent fit ($\chi^2/N_{\mathrm{DF}} = 1.22$), although at all energies the measured average shower multiplicities are somewhat closer to the NB than to the LN calculation, and the NB distributions give somewhat better fits than do the LN distributions. The phenomenological expression Eq. (2) and the negative binomial expression Eq. (3) therefore both provide excellent fits to the 525 GeV shower particle distributions, and the two-parameter log-normal form Eq. (6) is only slightly inferior. However, the distinction between the NB and LN forms could depend on the statistical size of the measured sample. In the largest data sets, 200 GeV pions and protons in Tables III and IV, the NB distribution appears to be preferred.

B. Pseudorapidity distributions

In Fig. 8 the shower particle pseudorapidity distributions are shown for inclusive events produced by pions at 60, 200, 300, and 525 GeV. Anzon *et al.* [11] have reported the presence of a two-peaked structure in the pseudorapidity distribution for 200 GeV pions. El-Nadi *et al.* [21] have also presented evidence for a bimodal pseudorapidity distribution; they see an effect for 340 GeV pions but *not* at 200 GeV. This effect does not occur in our other data samples—and particularly not at 525 GeV. Furthermore, the effect was not seen in the work by Babecki *et al.* [8] with 200 GeV pions. The 200 GeV bimodal peak reported by Anzon *et al.* [11] appears to be an experimental artifact. The 200 GeV pion pseudo-

TABLE III. Parameters obtained from fitting with negative binomial distribution.

Projectile	Energy (GeV)	$\langle n_s \rangle$	k	$D/\langle n_s \rangle$	χ^2	Number of points
π^-	525	15.54± 0.21	4.50± 0.25	0.54± 0.01	49.14	53
π^-	300	13.95± 0.18	4.05± 0.21	0.56± 0.01	51.08	49
π^-	200	12.23± 0.09	4.26± 0.14	0.56± 0.01	112.04	49
π^-	60	8.38± 0.19	5.05± 0.59	0.56± 0.02	23.43	26
p	800	19.57± 0.30	3.11± 0.15	0.61± 0.01	76.50	66
p	400	17.19± 0.41	3.03± 0.23	0.62± 0.10	33.48	50
p	200	13.84± 0.17	3.59± 0.17	0.59± 0.01	45.10	48
p	67	9.24± 0.18	4.23± 0.38	0.58± 0.07	25.30	30

TABLE IV. Parameters obtained from fitting with log-normal distribution.

Projectile	Energy (GeV)	σ	μ	$\langle n_s \rangle$	$D/\langle n_s \rangle$	χ^2	Number of points
π^-	525	0.56± 0.01	2.64± 0.01	16.40± 0.19	0.61± 0.01	61.99	53
π^-	300	0.57± 0.01	2.53± 0.01	14.75± 0.17	0.63± 0.01	82.65	49
π^-	200	0.53± 0.01	2.40± 0.01	12.70± 0.14	0.58± 0.01	269.29	49
π^-	60	0.54± 0.02	2.05± 0.02	8.93± 0.20	0.62± 0.02	34.70	28
p	800	0.63± 0.01	2.83± 0.02	20.73± 0.43	0.71± 0.01	99.54	66
p	400	0.66± 0.02	2.72± 0.02	18.94± 0.40	0.74± 0.03	48.30	50
p	200	0.59± 0.01	2.51± 0.01	14.58± 0.17	0.66± 0.01	100.63	48
p	67	0.56± 0.02	2.14± 0.02	9.94± 0.23	0.61± 0.02	61.32	30

rapidity distribution shown here is that of Babecki *et al.* There is a clear indication of limiting fragmentation in the target fragmentation region $\eta_{\rm lab} \leq 1$, where the distributions corresponding to the four beams overlap. The maximum pseudorapidity increases with energy, however, and the height of the plateau grows approximately as $\ln E_{\rm lab}$ (Fig. 8, insert). The former is a kinematic effect, while the latter is a dynamical effect expected to arise from scaling violation in the central region [22,23]. The measured 525 GeV pseudorapidity distribution is in good agreement with the FRITIOF prediction, as shown in Fig. 9.

In Fig. 10 the projectile fragmentation region is examined by making a translation to the projectile rest frame using

$$\eta' = \eta_{\rm lab} - \eta_{\rm beam} = \eta_{\rm lab} - \tanh^{-1}\beta, \qquad (8)$$

where β is the velocity of the incident pion. Again there is an overlap of the distributions, now in the region $\eta' > -4$.

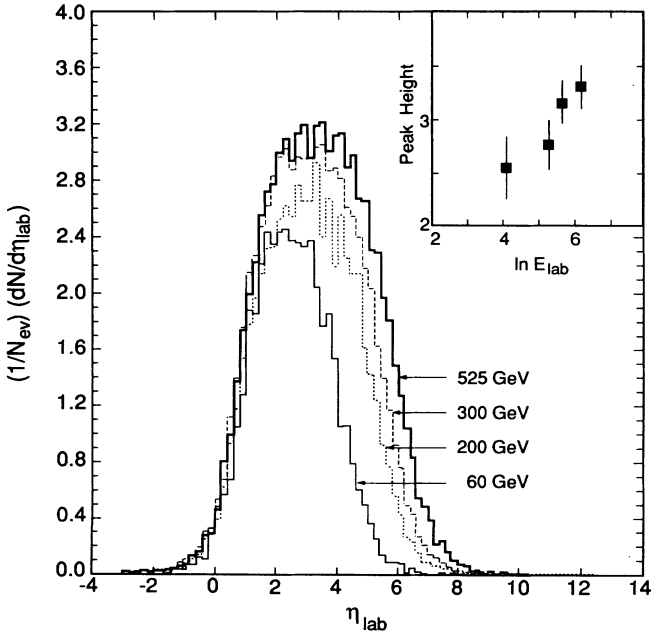

FIG. 8. Shower particle pseudorapidity distributions in laboratory frame for 60–525 GeV pions. Inset: Height of Gaussian fitted to pseudorapidity distribution vs $\ln E_{\rm lab}$.

The plots in Figs. 8 and 10 can be summarized as follows: The pseudorapidity distributions of charged particles produced in 60–525 GeV π-emulsion interactions are approximately independent of the beam energy in the target fragmentation region ($\eta_{\rm lab} \leq 1$) and the projectile fragmentation region ($\eta' > -4$). Thus, the energy dependence in $dN/d\eta$ is manifested mainly in the rise and broadening of the central pseudorapidity region.

Finally, the energy dependence of the average $\langle \eta \rangle$, the dispersion D_η, and the ratio $D_\eta/\langle \eta \rangle$ for 60–525 GeV pions is compared to 67–800 GeV protons in Fig. 11. The $\langle \eta \rangle$ and D_η increase with incident energy while $D_\eta/\langle \eta \rangle$ seems to decrease slightly. The pion behavior is essentially the same as that for high energy proton interactions.

IV. HEAVILY IONIZING PARTICLES

A. Multiplicity distributions

The multiplicity distributions of the heavy tracks from π^--emulsion interactions are shown in Fig. 12. Based on the data up to 300 GeV, Babecki *et al.* [8] concluded that the distributions do not vary significantly with the energy of the primary pion. Similarly, the distributions of heavy tracks seen in 67–800 GeV proton collisions have

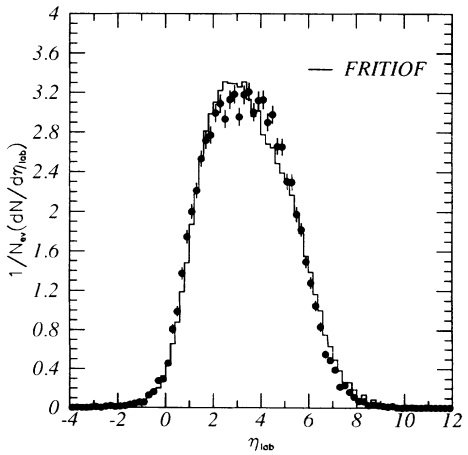

FIG. 9. Measured shower particle pseudorapidity distribution for 525 GeV pions (•) compared to FRITIOF Monte Carlo calculation.

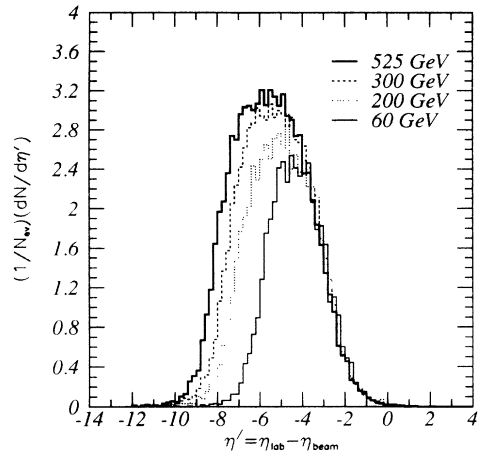

FIG. 10. The same as in Fig. 8 but in the pion rest frame.

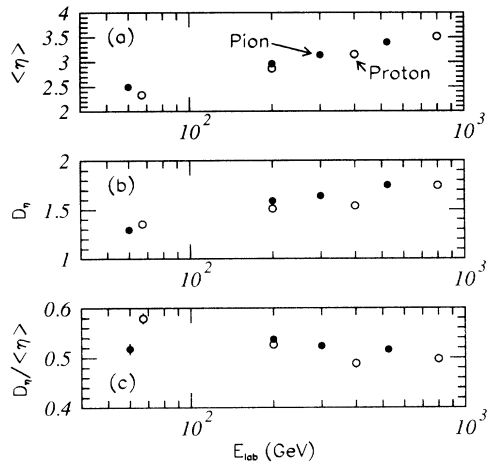

FIG. 11. Average value (a), dispersion (b), and the ratio of dispersion to the average (c) for shower particle pseudorapidity distributions as a function of the incident particle energy.

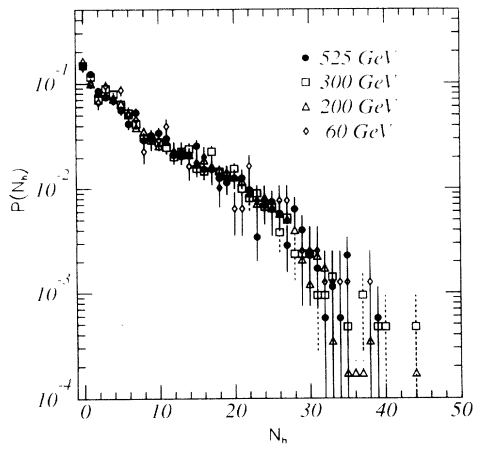

FIG. 12. $P(N_h)$ vs N_h for 60–525 GeV pions.

been found to be essentially energy independent [6]. The present results show no variation in the heavy track distribution with pion energy up to 525 GeV. The observed value of $\langle N_h\rangle = 7.0\pm0.2$ at 525 GeV is in excellent agreement with the values observed at lower energies (7.0 ± 0.2, 7.0 ± 0.1, and 7.1 ± 0.3 at 300, 200, and 60 GeV, respectively).

The KLM group has recently [24] demonstrated the presence of a saturation effect in $\langle N_b\rangle$ in high energy (200 GeV/nucleon) ^{16}O and ^{32}S interactions. In Fig. 13 we plot average $\langle N_b\rangle$ values versus N_g measured for 200 GeV proton and pion collisions, together with 200 GeV/nucleon ^{16}O and ^{32}S results. We see evidence of the same saturation of $\langle N_b\rangle$ for protons and pions as for the heavy nuclei. Figure 14 shows the result for 525 GeV pions, where a similar behavior is observed. Since N_b is a measure of the target excitation, it appears that the same number of grey tracks N_g (i.e., recoil protons) produces a similar degree of target excitation independent of the kind of projectile and the incident energy.

B. Angular distributions

The normalized $\cos\theta$ distribution of grey tracks for inclusive π^--emulsion interactions at 525 and 200 GeV are shown in Fig. 15, together with the distributions for 200 and 800 GeV protons and 200 GeV/nucleon ^{16}O and ^{32}S. In each case, the distributions are normalized to the total number of grey particles $N_{g,\mathrm{tot}}$ recorded in each sample. A similar graph is shown for black particles in Fig. 16. The grey track angular distributions are strongly peaked in the forward direction ($\cos\theta > 0$), while the corresponding distributions for black tracks exhibit little forward-backward asymmetry. If the target fragments are assumed to be predominantly protons whose velocities are given by a Maxwell-Boltzmann distribution, then based on a two-step vector model [25] the angular distribution is

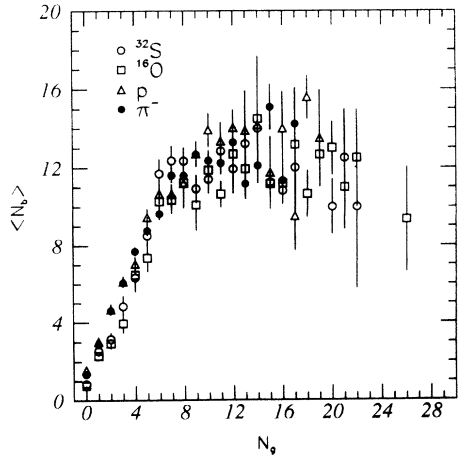

FIG. 13. $\langle N_b\rangle$ vs N_g for 200 GeV π and p and 200 GeV/nucleon ^{16}O and ^{32}S interactions.

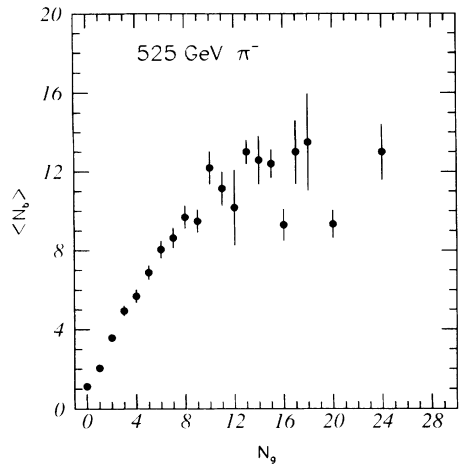

FIG. 14. $\langle N_b \rangle$ vs N_g for 525 GeV pions.

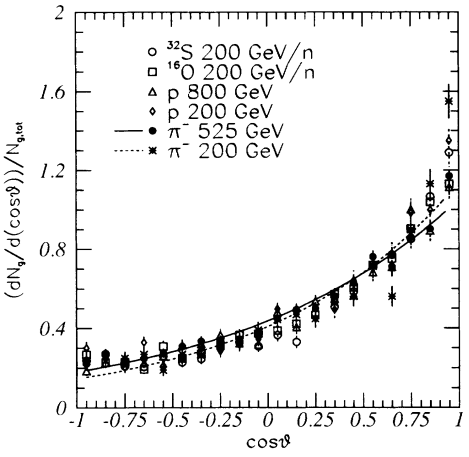

FIG. 15. Angular distribution of grey tracks for π, p, and heavy ion interactions in emulsion. The distributions are normalized to the total number of tracks $N_{g,\mathrm{tot}}$. Smooth curves are fits to two-step vector model [Eq. (9)] for 200 and 525 GeV pions.

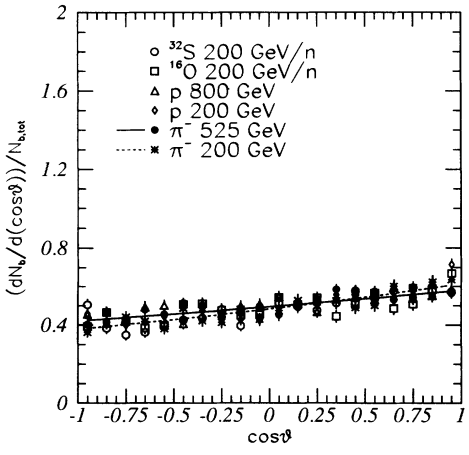

FIG. 16. Same as Fig. 15 for black tracks.

$$\frac{dN}{d\cos\theta} \propto \exp\left(\frac{4}{\sqrt{\pi}}\chi_0 \cos\theta\right), \tag{9}$$

where $\chi_0 = \beta_{\|}/\beta_0$; $\beta_{\|}$ is the longitudinal velocity of the center of mass of the fragmenting system and β_0 is the average velocity of the fragments in the center-of-mass system. The solid and dashed lines in Figs. 15 and 16 are the best fit angular distributions from Eq. (9) to the 525 GeV and 200 GeV π^- points, respectively. Two important conclusions can be drawn. First, the angular distributions of the grey and black tracks differ in shape, indicating that these tracks are created by particles originating from two different processes: the initial interaction and the subsequent evaporation of the excited target nucleus. Second, for the same target (i.e., emulsion), the angular distributions do not depend significantly on the type of projectile or its energy. Hence, the mechanisms of slow particle production appear to be the same in hadron-induced and heavy ion-induced interactions at different projectile energies.

The ratio of the average number of fragments in the forward to backward hemispheres is given by

$$\frac{\langle F \rangle}{\langle B \rangle} \propto \exp\left(\frac{4}{\sqrt{\pi}}\chi_0\right). \tag{10}$$

The forward-backward ratios obtained from Eq. (10) are compared to the data in Table V, where we also include $\langle F \rangle$, $\langle B \rangle$, and χ_0. The results for 200 and 800 GeV protons and for 200 GeV/nucleon ^{16}O and ^{32}S collisions are also listed in Table V for comparison. In all cases, the $\langle F \rangle / \langle B \rangle$ ratios decrease slightly with increasing projectile energy, although this decrease may be partially due to the uncertainties in the grey-black track identification (see Sec. II). If the black tracks are emitted by a stationary residual nucleus, we expect an isotropic distribution in Fig. 16. The curve in Fig. 16 is clearly not flat, however, implying $\beta_{\|} \neq 0$. If the typical fragmentation energy per nucleon is $E_0 \sim 6$–8 MeV, then $\beta_0 = (\frac{2E_0}{mc^2})^{1/2} \sim 0.1$ (assuming $m = m_n$) and $\beta_{\|} \lesssim 0.01$ for the residual nucleus system which produces the black tracks.

V. CORRELATION BETWEEN PARTICLE PRODUCTION AND FRAGMENTATION OF TARGET NUCLEI

Figure 17(a) shows the dependence of the average shower particle multiplicity on N_h. As the number of heavy tracks (i.e., the number of intranuclear collisions [26]) increases, the number of relativistic particles increases approximately linearly and then tends to saturate (at least at the highest pion energies). The solid curve drawn in Fig. 17(a) is the result of a three-parameter fit to the 525 GeV data, where the free parameters are the slope, intercept, and saturation level $\langle n_s \rangle_{\max} \sim 25.5$. Figures 17(b) and 17(c) show $\langle n_s \rangle$ for the 525 GeV pions as a function of N_g and N_b separately. In both cases the number of relativistic particles tends to bend over near $N_g \sim N_b \sim 8 - 12$. We note that $N_g \sim 8 - 12$ is approx-

TABLE V. $\langle F\rangle$, $\langle B\rangle$, $\langle F\rangle/\langle B\rangle$ and the velocity parameter χ_0.

Projectile	Energy	$\langle F\rangle$	$\langle B\rangle$	χ_0	$(F/B)_{\text{th}}$	$(F/B)_{\text{expt}}$
			Grey			
π^-	525	2.04± 0.06	0.86± 0.03	0.39	2.41	2.37 ± 0.11
π^-	200	1.54± 0.06	0.58± 0.03	0.45	2.78	2.66 ± 0.17
p	800	1.98± 0.07	0.80± 0.04	0.41	2.51	2.48 ± 0.15
p	200	1.92± 0.08	0.72± 0.04	0.45	2.78	2.67 ± 0.19
^{32}S	200	2.44± 0.10	0.91± 0.05	0.48	2.94	2.68 ± 0.18
^{16}O	200	2.50± 0.17	1.00± 0.06	0.43	2.65	2.50 ± 0.23
			Black			
π^-	525	2.22± 0.06	1.89± 0.05	0.07	1.17	1.17 ± 0.04
π^-	200	2.64± 0.09	1.97± 0.07	0.11	1.27	1.34 ± 0.07
p	800	2.45± 0.08	2.12± 0.08	0.07	1.16	1.16 ± 0.06
p	200	2.94± 0.10	2.18± 0.08	0.11	1.29	1.35 ± 0.07
^{32}S	200	2.67± 0.10	2.06± 0.08	0.11	1.28	1.30 ± 0.07
^{16}O	200	2.34± 0.10	1.95± 0.08	0.08	1.19	1.20 ± 0.07

imately the same place at which $\langle N_b\rangle$ tends to saturate as well in Fig. 14.

In order to understand the saturation in $\langle n_s\rangle$, we have estimated the maximum number of produced pions allowed by energy conservation. In a typical hadron-hadron interaction, the fraction of energy given up by the leading particle in the collision is given by the inelasticity $k \sim 0.5$. The maximum number of pions corresponds to the limiting case $k \to 1$ where none of the energy is carried off by the leading particles into either the target or the projectile fragmentation region, and the entire center of mass energy $\sqrt{s}$ is available for relativistic particle production. Essentially, we consider the limiting case of a thermodynamic fireball which evaporates to produce an isotropic distribution of relativistic produced particles in the center of momentum with total energy $\sqrt{s}$. We write the invariant cross section

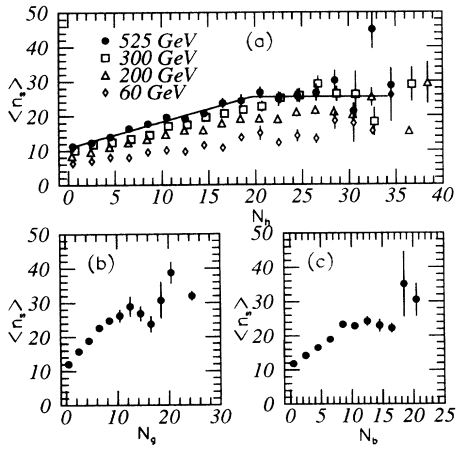

FIG. 17. (a): Average shower particle multiplicity vs numbers of heavy tracks N_h for 60–525 GeV pions. Curve is straight line fit to 525 GeV points with a saturation at $\langle n_s\rangle_{\max} = 25.5$. For clarity, the 200 and 300 GeV data points have been shifted slightly to the left and right respectively. (b) $\langle n_s\rangle$ vs N_g for 525 GeV pions. (c) $\langle n_s\rangle$ vs N_b for 525 GeV pions.

$$E\frac{d^3\sigma}{dp^3} = f_1(p_t)f_2(x) \tag{11}$$

as a product of a function f_1 of transverse momentum and a function f_2 of the Feynman x variable $x = 2p_\ell/\sqrt{s}$, where the transverse and longitudinal momenta in the c.m. frame are related by $p_t = p_\ell \tan\theta$. If we approximate f_1 as an exponential $e^{-\alpha p_t}$ with the same slope α (i.e., the same $\langle p_t\rangle$) for all x, and set the rapidity equal to the pseudorapidity η at high energies, then we can write the cross section in terms of the cm angular distribution $df/d(\cos\theta)$ as

$$d^2\sigma = Ae^{-\alpha p_t}\left(\frac{e^{-\eta}}{1+e^{-2\eta}}\right)^2 \frac{df}{d(\cos\theta)}dp_t d\eta. \tag{12}$$

Here A is a normalization constant.

We can now select particles at random with values of p_t and η chosen according to Eq. (12). The first particle can have a value of p_{t1} ranging from 0 to $\sqrt{s}/2$. The pseudorapidity can then be chosen in the range

$$-\eta_{\max} \le \eta_1 \le \eta_{\max}, \qquad \eta_{\max} = \frac{1}{2}\ln\frac{s}{p_{t1}^2 + m_\pi^2}. \tag{13}$$

Particle 1 therefore has longitudinal momentum

$$p_{\ell 1} = p_{t1}\frac{e^{2\eta_1}-1}{2e^{\eta_1}} \tag{14}$$

and total energy

$$E_1 = (p_{t1}^2 + p_{\ell 1}^2 + m_\pi^2)^{1/2}. \tag{15}$$

If the velocity β of the produced particle is greater than 0.7, the count of n_s is increased by 1. The available c.m. energy is decreased by E_1 and (if the remaining $\sqrt{s} > m_\pi$) a new p_t and η are chosen (now with a smaller $p_{t,\max}$ and a new value of $\eta_{\max}$). The process continues, with values of p_t and η being assigned from the distribution (12), as long as $\sqrt{s} > m_\pi$.

Since the produced particles are not necessarily all charged pions, we allow in the simulation for π^0, K

mesons, $p\bar{p}$, and $n\bar{n}$ using observed particle production ratios at energies reached at the CERN Intersecting Storage Rings (ISR) [23]. The only remaining adjustable parameter in the calculation is α, which is tuned so that the final $\langle p_t \rangle = 350$ MeV/c. With no additional free parameters, we can then count up the simulated number of relativistic secondaries with $\beta > 0.7$, starting with the initial value $\sqrt{s} = 31.4$ GeV. For an isotropic c.m. angular distribution, we find an average saturation level of relativistic secondaries $\langle n_s \rangle_{\max} = 31.1$, only slightly larger than the observed $\langle n_s \rangle_{\max} = 25.5$.

This simple kinematic argument[1] may partially explain the observations, but the statistical limitations of the data set must be recognized. It is interesting that, if the saturation in $\langle n_s \rangle$ in fact occurs at the point where no additional c.m. energy is available, then this point is reached, on average, at numbers of collisions corresponding to $N_g \sim 8-12$ and $N_h \sim 20$. The physical mechanism connecting heavy and relativistic particle production, if in fact such a connection exists, remains unknown.

Given the correlation of the shower particle multiplicity with the number of heavily ionizing tracks, we also look at the dependence of the shower particle pseudorapidity distributions on N_h. In Fig. 18 we present the dependence of the average pseudorapidity $\langle \eta_{\rm lab} \rangle$ of the shower particles on N_h for pion interactions at 60–525 GeV. One can see that with increasing N_h, the average pseudorapidity shifts toward lower values for all the primary energies. However, for large N_h this dependence levels off. In Fig. 19 we show the shower particle pseudorapidity distributions characterized by different N_g and N_b values at 525 GeV. We find a similar shift in the pseudorapidity distributions to the lower η values with increasing N_g or N_b. No drastic change in the shape of $dN/d\eta$ distributions is seen with the increase of N_g or N_b. However, in the interactions with large N_g (N_b), i.e., for large number of intranuclear collisions, the distributions become asymmetric, with more particles produced at low pseudorapidities.

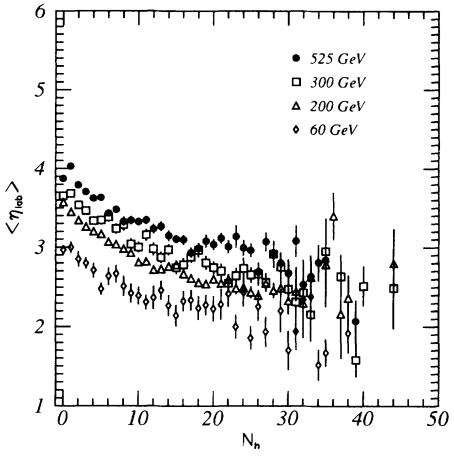

FIG. 18. Average pseudorapidity vs N_h.

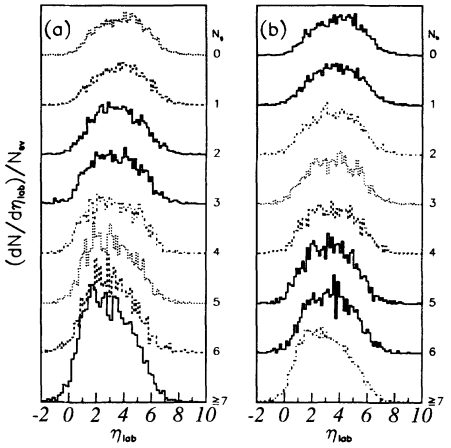

FIG. 19. 525 GeV pion shower particle pseudorapidity distributions for different values of N_g and N_b.

VI. CONCLUSIONS

We have compared the results of measurements of 525 GeV π^- interactions in emulsion with 60, 200, and 300 GeV π^- interactions and 67 – 800 GeV proton interactions in emulsion. Average shower particle multiplicities continue to follow roughly the same energy dependence seen at lower energies, with an essentially constant ratio $\langle n_s \rangle_p / \langle n_s \rangle_\pi \sim 1.1$ over the energy range 60–525 GeV and with a somewhat steeper slope than at low energies. The shape of the multiplicity distributions does not vary significantly with energy, and the ratio of the dispersion to the mean multiplicity is constant over the entire energy range for both pion and proton collisions. The multiplicity distributions are well fit by both the phenomenological expression (2) and a negative binomial distribution (and only slightly worse by a log-normal distribution). The predictions of the FRITIOF Monte Carlo code agree reasonably well with the measured 525 GeV π^- shower particle multiplicity and pseudorapidity distributions.

The average number of heavily ionizing tracks $\langle N_h \rangle$ remains the same at 525 GeV as at lower energies. $\langle N_b \rangle$ saturates with an increasing number of grey tracks N_g

[1] We have assumed an isotropic angular distribution in the c.m. in order to maximize $\langle n_s \rangle$. More realistically, the distribution has cylindrical symmetry reflecting the observation that a fraction of the energy is carried off by the leading particles into the fragmentation regions. If we model a cylindrical distribution by $\frac{df}{d(\cos\theta)} \sim \sin^{-m}\theta$, then $\langle n_s \rangle_{\max} = 28.2$ for $m = 1$, 25.8 for $m = 1.5$, and 22.6 for $m = 2$. As m increases from 0 to approximately 1.5 (i.e., as the distribution moves from isotropic to cylindrical), the agreement between calculated and observed average saturation levels becomes even closer.

(i.e., intranuclear collisions), and this effect seems to be independent of the type and energy of the projectile particle. The apparent observed saturation in $\langle n_s \rangle$ may be related to energy conservation in the particle production process. Finally, no indication is seen for any qualitatively different behavior in the 525 GeV pion data as compared to 60 – 300 GeV pions or 67 – 800 GeV protons interacting in emulsion.

[1] H. Satz, Annu. Rev. Nucl. Part. Sci. **35**, 245 (1985); K. Kajantie and L. McLerran, *ibid.* **37**, 293 (1987).
[2] A. Dabrowska *et al.*, Phys. Rev. D **47**, 1751 (1993).
[3] S. Fredriksson *et al.*, Phys. Rep. **144**, 187 (1987).
[4] J. Babecki *et al.*, Acta Phys. Pol. B **9**, 495 (1978).
[5] J. Babecki *et al.*, Phys. Lett. **47B**, 268 (1973); Acta Phys. Pol. B **5**, 315 (1974).
[6] A. Abduzhamilov *et al.*, Phys. Rev. D **35**, 3537 (1987); Y. A. Abdurazakova *et al.*, Acta Phys. Pol. B **18**, 249 (1987).
[7] A. Abduzhamilov *et al.*, Z. Phys. C **40**, 223 (1988).
[8] J. Babecki *et al.*, Acta Phys. Pol. B **16**, 323 (1985).
[9] R. Hołyński *et al.*, Z. Phys. C **31**, 467 (1986).
[10] E. V. Anzon *et al.*, Yad. Fiz. **22**, 736 (1975) [Sov. J. Nucl. Phys. **22**, 380 (1975)]; S. A. Azimov *et al.*, *ibid.* **26**, 346 (1977) [**26**, 180 (1977)]; Nuovo Cimento A **84**, 117 (1984).
[11] E. V. Anzon *et al.*, Nucl. Phys. **B129**, 205 (1977).
[12] E. G. Boos *et al.*, Nucl. Phys. **B143**, 232 (1978).
[13] A. Abduzhamilov *et al.*, Mod. Phys. Lett. A **3**, 489 (1987); E. G. Boos *et al.*, Nucl. Phys. **B137**, 37 (1978).
[14] T. F. Hoang *et al.*, Z. Phys. C **29**, 611 (1985); Particle Data Group, J. J. Hernández *et al.*, Phys. Lett. B **239**, 1 (1990).
[15] A. S. Carroll *et al.*, Phys. Lett. **80B**, 319 (1979).
[16] B. Andersson *et al.*, Phys. Rep. **97**, 31 (1983); B. Nilsson-Almqvist and E. Stenlund, Comput. Phys. Commun. **43**, 387 (1987); T. Sjöstrand, *ibid.* **39**, 347 (1986).
[17] Z. Koba, H. B. Nielsen, and P. Olesen, Nucl. Phys. **B40**, 317 (1972).
[18] A. Giovannini, Nuovo Cimento A **15**, 543 (1973); P. Carruthers and C. C. Shih, Phys. Lett. **125B**, 242 (1983); A. Giovannini and L. Van Hove, Z. Phys. C **30**, 391 (1986).
[19] R. Szwed *et al.*, Mod. Phys. Lett. A **5**, 1851 (1991); R. Szwed and G. Wrochna, Z. Phys. C **47**, 447 (1990).
[20] S. Carius and G. Ingelman, Phys. Lett. **27B**, 647 (1990).
[21] M. El-Nadi *et al.*, Phys. Rev. D **27**, 12 (1983); Nucl. Phys. **10**, 875 (1984).
[22] W. Busza and R. Ledoux, Annu. Rev. Nucl. Part. Sci. **38**, 119 (1988).
[23] G. Giacomelli, Int. J. Mod. Phys. A **5**, 223 (1990).
[24] A. Dabrowska *et al.*, Z. Phys. C **59**, 399 (1993).
[25] J. M. Alexander, in *Nuclear Chemistry*, edited by L. Yaffe (Academic, New York, 1968), Vol. I, p. 273; H. H. Heckman *et al.*, Phys. Rev. C **17**, 1651 (1978).
[26] B. Furmanska *et al.*, Acta Phys. Pol. B **8**, 973 (1977); E. Stenlund and I. Otterlund, Nucl. Phys. **B198**, 407 (1982).

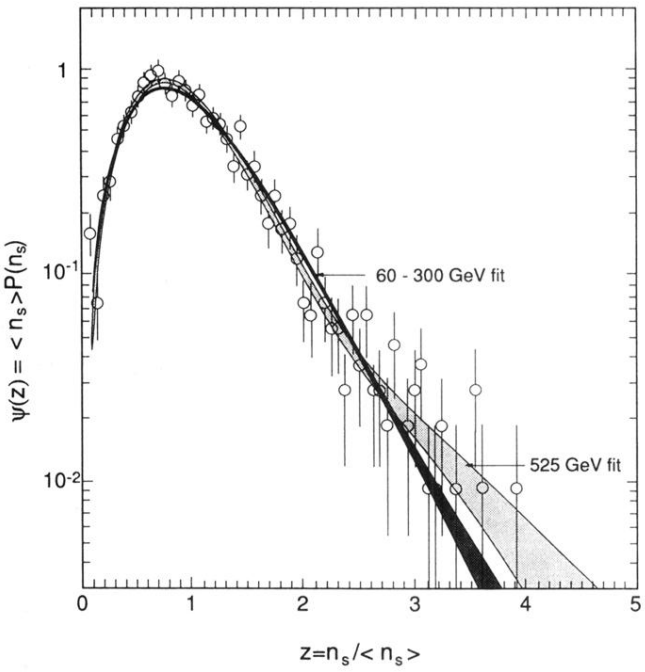

FIG. 6. $\psi(z)$ vs z for 525 GeV pions. The two bands represent fits to the 60–300 GeV π^- data of Ref. [8] and the 525 GeV data of the present work. The width of the bands corresponds to varying the individual fit parameters until $\chi^2/N_{\rm DF}$ increases by 1.